

Thermal Transport Properties of Water and Ice from one Single Experiment¹

U. Hammerschmidt²

¹ Paper presented at the Fourteenth Symposium on Thermophysical Properties, June 25-30, 2000, Boulder, Colorado, U.S.A.

² Physikalisch-Technische Bundesanstalt, Braunschweig, Bundesallee 100,
D-38116 Braunschweig

ABSTRACT

For the first time, the transient hot wire (THW) and the transient hot strip (THS) techniques were used to measure the thermal conductivity and thermal diffusivity of solid and the thermal conductivity of liquid H₂O simultaneously in one run. With the additional knowledge of the thermal diffusivity of water from a subsequent single phase run, the latent heat of melting can be determined as well as the time dependent position of the interface between both phases during an experiment. The results of the dual phase measurements are compared with those obtained in the single phase experiments using the same simple set up. The composite THS and THW signals are interpreted based on the underlying phase-change-theory of Stefan and Neumann, as outlined briefly in the text.

KEY WORDS: ice, latent heat, melting, phase transition, transient hot strip, transient hot wire, thermal conductivity, thermal diffusivity, water

1. INTRODUCTION

The Transient Hot Strip (THS-) method is known well as a fast technique to measure simultaneously the thermal conductivity and thermal diffusivity of solids [1]. For liquids, so far only Gustafsson et al. [2-5] and Groß et al. [6] reported on this technique.

State of the art for measuring both mentioned thermal transport properties of liquids is the Transient Hot Wire (THW-) technique (cf. e.g., [7], [8]). This closely related method uses a wire in place of the strip as the sensor. From this arrangement substantial advantages arise: First, the underlying mathematical model of the (one-dimensional) wire is not as complex as that of the (two-dimensional) strip and the corrections to it are much better understood. Secondly, the linearized THW model enables the isolation of non-conductive mechanisms of heat transfer such as convection. For fluids the THW method is accepted worldwide as the most accurate technique.

However, to set up a THW apparatus is a difficult and troublesome task: To meet the one-dimensional model, the radius of the wire has to be as thin as possible. It has to be maintained straight and under slight tension but without stretching it. Moreover, a complex peripheral instrumentation is needed for the most precise THW cells which consist of two wires of different length in a Wheatstone bridge arrangement. This circuit has to be adjusted and operated thoroughly. By contrast, the strip of a THS experiment is easily to be fixed within a measuring cell (cf. Fig. 2). Moreover, the width of the strip may be chosen out of a relatively wide range up to 12 mm. The strip works properly in a simple four wire circuit, to be connected to a DVM and a constant current source only. Moreover, as Groß et al. noted in [5], the electrical conductivity of a substance under test may be greater by two orders of magnitude than for the THW method, because of the strip's larger ratio of cross section and length. From the same geometrical reasons, the onset of convection can be significantly later than in a THW experiment because of the smaller heat flow density at the surface of the strip (cf. sect. 3.)

However, within the framework of the THS nonlinear mathematical model the nonlinear phenomena convection could not be detected. This major drawback of the THS method for fluids can now be circumvented by evaluating the THS signal by the recently developed linearized model [9] or by a combination of this procedure with the nonlinear estimator [10]. On the basis of the linear approximation, a new experimental attempt has been made to implement the THS method to a liquid. Water was taken as the sample for two reasons: First, its thermal transport properties are known well [11], [12] and, secondly, water can easily be measured in the solid state too.

After a brief review of the THW and THS models, the present paper deals with measurements of the thermal conductivity and thermal diffusivity of H₂O at temperatures from -20 °C to +20 °C. Composite THS and THW signals are presented which were observed while the sample changes its phase at the freezing point, induced by the heat liberated from the strip or the wire. From these signals the thermal transport coefficients can be derived simultaneously for the liquid and the solid state around 0 °C.

Till now, the theory of heat conduction with progressive melting is derived for planar, line (THW), and spherical heat sources only. To analyze our THS signals, a specific approximation to the line source solution was derived.

2. THEORY

A line or semiinfinite strip heat source of specific strength $\Phi/L = \text{const.}$ is surrounded by a dielectric initially at uniform temperature $T = T_0$. The resulting time dependent temperature rise at a cylindrical surface at a distance r from the reference axis ($r = 0$) is governed by:

$$\Delta T(t) = T(t) - T_0 = \frac{\Phi}{2\sqrt{\pi L \lambda}} \cdot f(\tau(r, t, a)) \quad (1)$$

The signal $\Delta T(t)$ is a measure of the thermal conductivity λ and thermal diffusivity a of the sample (e.g., [1], [7]). In a transient hot wire (THW) and transient hot strip (THS) experiment the temperature excursion $T(t)$ is monitored in time t as the voltage drop $U(T(t))$ across a current-carrying metal wire of radius $r = r_0 \rightarrow 0$ or strip of thickness $v \rightarrow 0$ and width D

$$U(T(t)) = U_0 \left(1 + \alpha \frac{U_0 I}{2\sqrt{\pi} L \lambda} \cdot f(\tau) \right) \quad (2)$$

The initial voltage drop U_0 is observed at time zero. α denotes the temperature coefficient of the electrical resistance of the sensor (wire or strip) of length L . $f(\tau)$ specifies the shape of the signal and is called the sensor function. For a wire, $f(\tau)$ reads

$$f(\tau) = f(\tau_r) = -\frac{1}{\sqrt{4\pi}} \text{Ei}(-\tau_r^{-2}) \quad (3)$$

where the nondimensional time is defined by

$$\tau_r = \frac{\sqrt{4at}}{r_0}. \quad (4)$$

For a strip

$$f(\tau) = f(\tau_D) = \tau_D \text{erf}(\tau_D^{-1}) - \frac{\tau_D^2}{\sqrt{4\pi}} [1 - \exp(-\tau_D^{-2})] - \frac{1}{\sqrt{4\pi}} \text{Ei}(-\tau_D^{-2}) \quad (5)$$

is valid where

$$\tau_D = \frac{\sqrt{4at}}{D}. \quad (6)$$

Both sensor functions are nonlinear and implicit in real time t . For practical purposes ($\tau^{-2} \ll 1$), first-order approximations which are linear in $\ln t$ can be obtained. They are based on the related series expansions of Eq. (3) and Eq. (5), respectively. $f(\tau_r)$ can be expressed as

$$f(\tau_r) \approx \frac{1}{2\sqrt{\pi}} (-\gamma + \ln \tau_r^2). \quad (7)$$

Here, $\gamma = 0.5772\dots$ (Euler's constant). In the case of the THS technique, the quasilinear approximation

$$f(\tau_D) \approx \frac{1}{2\sqrt{\pi}} (3 - \gamma + \ln \tau_D^2) \quad (8)$$

is valid. Substitution of Eq. (7) and Eq. (8), respectively, into Eq. (2) results in

$$\Delta U^W(t) = U^W(t) - U_0^W \approx \frac{\alpha(U_0^W)^2 I}{4\pi L \lambda} \left(\ln t + \ln \frac{4a}{C r_0^2} \right) = m^W t' + n^W \quad (9)$$

for the THW method (superscript "W") and

$$\Delta U^S(t) = U^S(t) - U_0^S \approx \frac{\alpha(U_0^S)^2 I}{4\pi L \lambda} \left(3 + \ln t + \ln \frac{4a}{C D^2} \right) = m^S t' + n^S. \quad (10)$$

for the THS technique (superscript "S"). Here, $C = \exp \gamma$. In both cases, the expression that governs the slope of the line segment, m , takes the form $m = \alpha U_0^2 I / 4\pi L \lambda$. The intercept is given with $n^W = m^W \ln(4a / C r_0^2)$ for a wire and $n_D = m^S (3 + \ln 4a / C D^2)$ for a strip. From these coefficients both measurands follow as

$$\lambda = \frac{\alpha U_0^2 I}{4\pi L m} \quad (11)$$

and

$$a = \frac{C r_0^2}{4} \exp\left(\frac{n^W}{m^W}\right) = \frac{r_0^2}{2.25} \exp\left(\frac{n^W}{m^W}\right) \quad (12)$$

or

$$a = \frac{C D^2}{4} \exp\left(\frac{n^S}{m^S} - 3\right) = \frac{D^2}{45} \exp\left(\frac{n^S}{m^S}\right) \quad (13)$$

The ideal model, Eq. (1) is valid for all times because of an unbounded sample. In practice, the valid time domain of Eq. (1) is set at its lower end, t_{\min} , by the characteristic length of the sensor, $r = r_0$ and $r = D$, respectively and at its upper end, t_{\max} , by the finite outer radius $r = R_0$ of the cylindrical sample. The available measurement time $[t_{\min}, t_{\max}]$ can be located by the upper and lower curved portions of the temperature vs \ln time graph. For small times, all data points which deviate by more than $\varepsilon = 0.5\%$ from the ideal straight line fit are discarded from all subsequent analysis. Therefore, the lower end point is set to be $\tau_{r(\min)} = 6$ for the wire [14] and $\tau_{D(\min)} = 2$ for the strip [9]. It then follows from Eqs. (4) and (6), respectively, that a linear segment does not start in real time before

$$t_{\min}^W \geq \frac{9r_0^2}{a} \quad (14)$$

and

$$t_{\min}^S \geq \frac{D^2}{a}, \quad (15)$$

repectively. For both techniques, the upper end point t_{\max} is proportional to the ratio of the square of the outer radius $r = R_0$ to the thermal diffusivity a [15, 16]:

$$t_{\max} < c \frac{R_0^2}{a} \quad (16)$$

For the THW technique, the constant c has to be chosen out of the range $0.17 < c(\varepsilon) < C/4$ depending on the approximation error ε [15]. A finite elements analysis performed recently [16], confirms this c -range. Furthermore, as long as $R_0 \geq 3D$, the range mentioned is valid for the time t_{\max}^S of THS signals too. Correspondingly for both techniques, it is found, that $c = 0.2$ causes a deviation $\varepsilon = 0.5\%$.

From a formal point of view, the working equations of the THS and THW methods, Eqs. (9) and (10), are very closely related. Substituting the linearized THS-sensor function, Eq. (8), into Eq. (1) and assuming that $U_0^W = U_0^S$ and $r_0 = D$ one obtains for the temperature rise of the strip

$$T^S(t) \approx T_0 + \frac{U_0 I}{4\pi L \lambda} \left(3 + \ln t + \ln \frac{4a}{CD^2} \right) = T_0 + \frac{U_0 I}{4\pi L \lambda} \ln \frac{4at}{CD^2} + 3 \frac{U_0 I}{4\pi L \lambda} = T_0 + T_c + T^W(t) \quad (17)$$

where $T_c = \text{const.}$ From the right hand side of Eq. (17) it is obvious that the THS signal is equal to the THW signal plus the constant offset-temperature T_c . Considering a line heat source at $r = 0$ for both techniques, the virtual temperature station is at $r = r_0$ for the THW method and at $r = D$ for the THS technique. In other words, the linearized electrical signal of the strip, may be interpreted like a THW signal that is shifted by a constant offset voltage $U_{\text{off}} = 3\alpha U_0^2 I / 4\pi L \lambda$. This effect alters the intercept n , however, it does not alter the slope m (cf. Eq. (11)).

2.1. Phase-Change Problem

Unlike steady state techniques which operate at a constant working temperature, T_W , transient methods to determine the thermal conductivity involve a time dependent increase in temperature of the sample. This temperature rise can be used to induce a phase transition of the sample during a run while measuring its thermal transport properties λ and a of H_2O .

The theoretical analysis of heat conduction with progressive freezing or melting is very difficult because of the moving interface between the solid and the liquid phases. Here, latent heat, H , is absorbed or liberated permanently. Stefan [17] was the first to discuss the problem of the formation of ice by a planar heat sink (“Stefan’s problem”). Neumann [18] solved this two-phase problem exactly and in closed form. For a line heat sink of constant strength Φ/L , as mentioned above, a solution is given by e.g. Özisik [19]. His analysis of a one-dimensional transient phase-change problem can be taken as a basis for our two-phase problem of a strip heat source.

As has already been shown above, for a given time window $[t_{\min}, t_{\max}]$, the strip heat source acts most similar to a line source. Therefore, first Özisik’s heat sink solution has to be transformed to a heat source solution, and, secondly, it has to be rearranged formally to a working equation for THS conditions that applies to our experimental results. Hence, it is sufficient here to solve the phase-change problem for the simpler arrangement of a line heat source as specified in sect. 2. Here, T_0 is significantly lower than the melting temperature T_M .

The solution, $T(r, t)$, can be found by specifying the two physically distinct parts of the system (solid, liquid) by individual Fourier field equations. Two phases are *initially* present:

$$\text{liquid: } \frac{1}{r} \frac{\partial}{\partial r} \left(r \frac{\partial T_L}{\partial r} \right) = \frac{1}{a_L} \frac{\partial T_L}{\partial t} \quad \text{in} \quad 0 < r < s(t), t > 0 \quad (18)$$

$$\text{solid: } \frac{1}{r} \frac{\partial}{\partial r} \left(r \frac{\partial T_S}{\partial r} \right) = \frac{1}{a_S} \frac{\partial T_S}{\partial t} \quad \text{in} \quad s(t) < r < \infty, t > 0 \quad (19)$$

All quantities pertaining to the liquid and to the solid are denoted by subscripts "L" and "S", respectively. $r = s(t)$ is the time-dependent position of the moving boundary (interface). Eqs. (18) and (19) do not include neither natural convection nor heat transport by the hydrodynamic flow of the liquid due to the difference in density between ice and water. Both effects do not interfere significantly during the experimental runs. The nature of the problem involves the following boundary conditions:

$$T_S(r, t) \rightarrow T_0 \quad \text{as} \quad r \rightarrow \infty, t > 0 \quad (20)$$

$$T_S(r, t) = T_0 \quad \text{as} \quad t = 0, \text{ in } r > 0 \quad (21)$$

On the interface, temperatures of both phases are equal to the melting temperature, T_M :

$$T_S(r, t) = T_L(r, t) = T_M \quad \text{at} \quad r = s(t), t > 0 \quad (22)$$

Here, at $s(t)$, the nonlinear heat balance can be written as

$$\lambda_L \frac{\partial T_L}{\partial r} - \lambda_S \frac{\partial T_S}{\partial r} = \rho H \frac{ds(t)}{dt} \quad \text{at} \quad r = s(t), t > 0 \quad (23)$$

As mentioned, the densities of the liquid, ρ_L , and the solid phase, ρ_S , are considered to be uniform, $\rho_L = \rho_S = \rho$. H denotes the specific latent heat of melting which is continuously absorbed at the progressing interface. Already in Neumann's derivation, it is pointed out that for the solution to satisfy the conditions for all time, this position had to be given by

$$s(t) = 2\delta \sqrt{a_L t} \quad (24)$$

where δ is a proportionality constant. Eqs. (18) and (19) are satisfied by:

$$T_L(r, t) = T_M - \frac{\Phi}{4\pi L \lambda_L} \left[\text{Ei} \left(-\frac{r^2}{4a_L t} \right) - \text{Ei}(-\delta^2) \right] \quad \text{in} \quad 0 < r < s(t) \quad (25)$$

$$T_S(r, t) = T_0 - \frac{T_0 - T_M}{\text{Ei} \left(-\delta^2 \frac{a_L}{a_S} \right)} \text{Ei} \left(-\frac{r^2}{4a_S t} \right) \quad \text{in} \quad s(t) < r < \infty \quad (26)$$

The constant δ can be obtained when Eqs. (25) and (26) are introduced into the interface balance equation (Eq. (23)).

$$\frac{\Phi}{4\pi L} \exp(-\delta^2) + \frac{\lambda_s(T_M - T_0)}{\text{Ei}\left(-\delta^2 \frac{a_L}{a_s}\right)} \exp\left(-\delta^2 \frac{a_L}{a_s}\right) = \delta^2 a_L \rho H \quad (27)$$

This transcendental relation has to be solved in graphical form. Eqs. (25) and (26) reduce to their basic form, respectively, for opposite cases of $s(t)$:

$$T_L(r, t) = T_M - \frac{\Phi}{4\pi L \lambda_L} \text{Ei}\left(-\frac{r^2}{4a_L t}\right) \quad \text{in} \quad s(t) \rightarrow \infty \quad (28)$$

because δ also tends to infinity and $-\text{Ei}(-\delta^2) \rightarrow 0$. Rearranging Eq. (29) results in

$$C = -\frac{(T_0 - T_M)}{\text{Ei}\left(-\delta^2 \frac{a_L}{a_s}\right)} = \frac{\delta^2 a_L \rho H - \frac{\Phi}{4\pi L} \exp(-\delta^2)}{\lambda_s \exp\left(-\delta^2 \frac{a_L}{a_s}\right)} \quad (29)$$

For $s(t) \rightarrow 0$, δ vanishes too. Thus, the right hand side of Eq. (29) becomes $C = -\Phi/4\pi L \lambda_s$ and Eq. (26) reduces to:

$$T_s(r, t) = T_0 - \frac{\Phi}{4\pi L \lambda_s} \text{Ei}\left(-\frac{r^2}{4a_s t}\right) \quad \text{in} \quad s(t) \rightarrow 0 \quad (30)$$

The two cases of one-phase and two-phase systems are shown in graphical form in Fig. 1. Both parts of the curve denoted "2-phase system" were calculated for the same r value.

As will be shown later (cf. section 3.), our basic experiments are governed by Eq. (25) which is valid for the "inner range". Here, the temperature station is virtually located at $0 < r = D < s(t)$ for the strip and $0 < r = r_0 < s(t)$ for the wire. The boundary condition involved is given with Eqs. (22) and (23). It is the situation of a "progressing (outer) isothermal boundary" ($T = T_M = \text{const.}$) which is continuously driven outward by the heat flow emitted by the wire, practically as long as $t \leq t_{\max}$.

As has been done to Eqs. (3) and (5), Eqs. (25) may be approximated to

$$T_L(r, t) = T_M - \frac{\Phi}{4\pi L \lambda_L} \left[\gamma + \ln\left(\frac{4a_L t}{r^2}\right) + \tilde{\delta} \right] \quad (31)$$

$$T_L(t) - T_M = \Delta' T(t) \approx \frac{U_0 I}{4\pi L \lambda_L} \left(\ln t + \ln \frac{4a_L}{Cr_0^2} + \tilde{\delta} \right) \quad (32)$$

The line segment of the THW voltage signal is specified by

$$U^w(T(t)) - U^w(T_M) \approx \frac{\alpha(U_0^w)^2 I}{4\pi L \lambda} \left(\ln t + \ln \frac{4a_L}{Cr_0^2} + \tilde{\delta} \right) = m^w t' + \tilde{n}^w \quad (33)$$

Here, $\tilde{\delta} = -\text{Ei}(-\delta^2) = \text{const.}$ and $U^w(T_M) = \text{const.}$. Slope m^w and intercept \tilde{n}^w are specified by $m^w = \alpha(U_0^w)^2 I / 4\pi L \lambda$ and $\tilde{n}^w = m^w (\tilde{\delta} + \ln 4a/Cr_0^2)$. Hence, thermal conductivity λ and thermal diffusivity a of the liquid phase are then

$$\lambda_L = \frac{\alpha(U_0^w)^2 I}{4\pi L m^w} \quad (34)$$

$$a_L = \frac{Cr_0^2}{4} \exp\left[\frac{\tilde{n}^w}{m^w} - \tilde{\delta}(H)\right] \quad (35)$$

Obviously, the determination of λ_L from a THW phase change experiment is not affected by the latent heat, H . However, in the case of the thermal diffusivity it is. Physically, the thermal diffusivity can be considered as the ratio of the energy conducted to the energy stored per unit volume. While the energy conducted, $\Phi = \text{const.}$, is not altered by the phase change, the stored energy is increased during melting because of the latent heat per unit volume, $(-\rho H)$.

Additional experimnts were performed by the simultaneous use of a second temperature station which is fixed 10 mm apart from the hot wire or hot strip (cf. Fig. 2). This "cold wire" can sense within the "outer range", $s(t) < r = R_1 < \infty$, where the temperature $T_S(r, t)$ is governed by Eq. (26). Here, it is the situation of a "progressing inner isothermal boundary" ($T = T_M = \text{const.}$) which is continuously driven from the center against the cold wire. Eq. (26) may be approximated to

$$U^w(T(t)) - U_0^w \approx -\frac{U_0^w - U^w(T_M)}{\hat{\delta}} \left(\ln t + \ln \frac{4a_s}{CR_1} \right) = \hat{m}^w t' + n^w \quad (36)$$

provided $CR_1/4a_s t \ll 1$. It now follows for the amplitude factor $\hat{\delta} = \text{Ei}\left(-\delta^2 \frac{a_L}{a_s}\right)$

$$\hat{\delta} = \frac{U_0^w - U^w(T_M)}{\hat{m}^w} \quad (37)$$

and for the thermal diffusivity of the solid phase

$$a_s = \frac{CR_1}{4} \exp\left(\frac{n^w}{\hat{m}^w}\right) \quad (38)$$

So far, the phase-change problem has been solved for a line heat source. From formal considerations, it can be shown that

$$U^s(T(t)) - U^s(T_M) \approx \frac{\alpha(U_0^s)^2 I}{4\pi L \lambda} \left(3 + \ln t + \ln \frac{4a_L}{CD^2} + \tilde{\delta} \right) = m^s t' + \tilde{n}^s \quad (39)$$

is the approximate solution for a THS experiment which corresponds to Eq. (33). The measurands are to be evaluated from

$$\lambda_L = \frac{\alpha(U_0^s)^2 I}{4\pi L m^s} \quad (40)$$

and

$$a_L = \frac{CD^2}{4} \exp\left[\frac{\tilde{n}^s}{m^s} - 3 - \tilde{\delta}(H)\right] \quad (41)$$

3. EXPERIMENTS

The experiments were performed on the triply distilled deionised normal water/ice system at atmospheric pressure and temperatures between -20 °C and $+20$ °C. Before measuring, the water was boiled for several minutes to remove dissolved air from the liquid.

The sample is contained in a tubular cell made from stainless steel. The volume change that accompanies the phase change was accommodated by filling the cell with water only up to the flange (e). Then, a reservoir (f) remains for the excess of H_2O during freezing. This arrangement prevents the development of destructive pressures during freezing. The intake or outflow of water to or from the metering region during a run is exceedingly slow and generally does not disturb the heat transfer pattern inside.

The cell has a length of 210 mm and an inner radius $R_0 = 25$ mm (Fig. 2). (There is another cell made from plastics having the same length but a greater inner radius of $R_0 = 45$ mm. We used it to verify for the upper end time t_{\max} and to detect the onset of convection.) Parallel to the longitudinal axis of each tube, a Platinum strip (d) of 125 mm length, 3 mm width, and 0.01 mm thickness is mounted. Optionally, a wire of the same length and a radius $r_0 = 0.125$ mm can be fixed. The current sensor is maintained straight by four tensioning springs (stainless steel) (b) which themselves are supported by lead-throughs (a). Each lead-through additionally acts as a voltage or current terminal for the four wire electrical circuit of the sensor (single sensor measurements). At a precisely adjusted distance of $r = r_1 = 10$ mm from the longitudinal cell axis, the "cold wire" (g) of radius $r_0 = 0.125$ mm can be mounted. Its purpose is to measure the temperature at a known position between the main sensor and the container wall (dual sensor measurements). Both sensors are connected to their nanovoltmeter and constant current source. The current sources also operate as measuring devices. All four instruments are controlled by a PC. A calibrated platinum resistor Pt 100 measures the working temperature to ± 0.01 K. The cell is completely immersed in a thermostated bath that controls the fluid temperature to ± 0.1 K.

The most important advantage of a hot strip instead of a hot wire as the main sensor is its greater mechanical strength. The wire "survives" at most three cycles of freezing, melting and freezing before it is broken while the strip endures more than 20.

Beginning at time zero, a constant electrical current I out of the range from 0.8 to 1.5 A for the wire and up to 5 A for the strip is passed through the sensor while the voltage drop is recorded at a sampling rate of 14 s^{-1} .

For the single phase measurements, the current is adjusted so that the maximum temperature rise of the strip does not exceed 2 K. For each constant working temperature T_w and strip/wire current I , three successive runs were performed. Each data set, $\Delta U(t_i)|_{I, T_w}$, was then analysed and the mean value taken as the result. The evaluation of the THS data on ice follows the linear procedure (LP) as described briefly above and in some length in [9]. A typical THS signal plot, showing the strip's excess temperature vs the natural logarithm of time ($\ln t$), is given with Fig. 3 for ice at -5 °C. The signal can be divided into three distinct intervals, two outer curved ones, indicated as "S1" and "S3", and an inner linear one, "S2". The latter interval begins

at $t_{\min}^i = D^2/a_s = 9/1.2 = 7.5$ s and ends at $t_{\max}^i = 0.2R_0^2/a_s = 0.2 \cdot 45^2/1.2 = 337.5$ s. This segment of slope m and intercept n is taken to evaluate the thermal transport properties λ and a of the sample from Eqs. (11) and (13). For both nonlinear segments “S1” and “S3”, the approximation, Eq. (10), does not apply. In a similar manner, this behaviour can be observed for practically any effect that is not linear in $\ln t$, e.g., in the case of a fluid, convection (cf. Figs. 4 and 5). In contrast to the THS signals obtained on ice, those monitored on water had to be analysed by the Levenberg-Marquardt (LM) nonlinear regression procedure [10] for the following reason: Within the temperature range covered, the thermal diffusivity of ice is $a_s \approx 1.2 \text{ mm}^2\text{s}^{-1}$ while for water this transport property is smaller by one magnitude, $a_L \approx 0.1 \text{ mm}^2\text{s}^{-1}$. For the lower and upper end point of the linear signal segment, it follows from Eqs. (15) and (16) that for ice $t_{\min}^i \approx 7.5$ s and $t_{\max}^i \approx 337$ s (cf. Fig. 3) whereas for water $t_{\min}^w \approx 90$ s and $t_{\max}^w \approx 4000$ s. The latter result is valid for ideal conditions only, i.e. at the absence of convection. However, we observed the onset of convection e.g., at $T = 5$ °C at $t_{\text{conv}}^S \approx 30$ s for the THS technique (Fig. 4). Since $t_{\text{conv}} < t_{\min}^w$, those signals can not be analysed by the linear method. For the THW technique, the onset of convection at $T = 5$ °C is at $t_{\text{conv}}^w \approx 10$ s (Fig. 5, incl. undisturbed cold wire signal). But, here, the line segment begins earlier because $r_0 \ll D$, (cf. Eqs. (14) and (15)).

All dual phase runs were started on ice at a constant uniform working temperature, T_w . A constant current was fed to the sensor, large enough (1.) to induce a phase transition after at least 10 s and (2.) to subsequently produce a linear signal portion of sufficient length on water.

The ISO standard uncertainty of a THS measurement on dielectric solids like e.g., ice has recently been assessed [14]. The results differ only slightly for the linear and the nonlinear evaluation procedure. For the thermal conductivity the value $2u^S(\lambda) = 4.8\%$ was found while for the thermal diffusivity $2u(a) = 22\%$ is valid. For the ISO uncertainty of the THW method on solids, a paper is to be submitted ($2u^S(\lambda) = 5.2\%$). So far, the THS and THW ISO uncertainties for our measurements on fluids have not been assessed yet (cf. Fig. 6). As a first estimation, the above mentioned values can be adopted.

4. RESULTS

4.1. Single Phase Measurements

Prior to the dual phase measurements, single phase runs on H₂O were performed to check the validity of our THS set up, especially for fluids. Figs. 6 and 8 represent the results on the thermal conductivity and thermal diffusivity, respectively. Both transport properties are plotted vs temperature between -20 and 20 °C. Each diagram additionally shows comparative results from literature: Concerning the thermal conductivity, the guarded hot plate (GHP) data of Touloukian et al. [11] were additionally plotted along with the transient hot wire (THW) data of Ratcliffe [12] and Ramirez et al. [13]. The latter claim an uncertainty of 0.5 % for their new standard reference data set on liquid H₂O. Graphical comparison is made with reference data sets in Fig. 7. For ice the maximum deviation from our data is -1.22 % whereas for water the departure does not exceed 0.7 %. This is an excellent result regarding our above mentioned uncertainties.

For the thermal diffusivity, the ISO uncertainty ($2u$) of our instrument is not better than 22 % for solids (error bars in Fig. 8) [11]. Accordingly, our data set on ice diverges significantly from those of Touloukian et al. [12] and James [15]. James stated an uncertainty of 7 % (error bars in Fig. 8) for his data on solid and liquid water. Nevertheless, for liquid water a deviation of 6.5 % in maximum of our data from the others is fairly good for a thermal diffusivity data set originating from THS measurements.

4.2. Dual Phase Measurements

As has been outlined first in [9] the linearized THS method is capable of measuring the thermal transport properties of composite media consisting of two layers having an interface at a fixed position but of transient temperature. A two-phase system like water and ice can be treated as a composite media too, however, here the interface has a fixed temperature but it moves. It is that characteristic of a two phase composite media which allows to solve the underlying differential equation in closed form (cf. sect. 2.1.).

H₂O has been taken as the sample fluid for the reasons outlined in sect. 1. Furthermore, for these first experiments, it was very important to select a substance of only slightly varying thermal transport properties over the range ($-5 \leq T_M / ^\circ\text{C} \leq 15$). Dual phase measurements were carried out using the THS method in single sensor mode, (dual sensor mode THS experiments are planned) and the THW technique in dual sensor mode (hot and cold wires).

A typical composite THS signal is shown in Fig. 9. Fig. 12 represents a typical THW signal where the cold wire signal is additionally plotted (dual sensor measurement).

For the THS signal (Fig. 9), the working temperature is -3°C and the constant current I fed to the strip is 5 A. This combination leads, after 13 s of heating the ice (linear segment: "L1"), to a maximum excess temperature of the strip just at the transition temperature. Now, melting of the sample is initiated from the hottest part of the strip, its centre, and propagates up and downwards along the longitudinal axis of the strip and to its edges. At the latest, at $t_{L(\min)} = 180$ s, the strip is completely immersed within a cylinder of water of radius $r \approx D$. At this fictitious nondimensional time $\tau_f = 2$ (cf. sect. 4.2.1. for "melt-lag"), the second linear segment ("L2") commences. It does not end before the thermal wave front reaches the container walls. The signal segment between the two linear portions "L1" and "L2" can precisely be expressed in terms of a polynomial of second degree in time ("P").

By playing with the working temperature and/or the electric current $I \propto \Phi$, fed to the sensor, one can perform THS and THW experiments in which the heat liberated by the current sensor induces and maintains a melting of the ice or another material. For ice, this has been done for different combinations of temperature and/or current, (Fig. 10).

4.2.1. Evaluation of Single Sensor Signals

To illustrate the analysis of a composite THS/THW single sensor signal on H₂O, Fig. 11 was calculated using the theory as outlined above. The dashed curve (denoted "water"), starting at $T_w = 0^\circ\text{C}$, indicates the signal of a single phase measurement on water, Eq. (2). The signal of the same measurement on a solid substance like ice (but having no phase transition) is represented with the solid/dotted curve (denoted "ICE" and "ICE cont."), starting at $T_w = -5^\circ\text{C}$, Eq. (2).

The dotted/solid curve, starting at $T_w = -1.8^\circ\text{C}$, (denoted "ice-water (cont.)", and "ice-water") shows the signal of a two phase measurement on H₂O where the solid, Eq. (26), and the liquid, Eq. (25), phases are initially present. The solid/solid curve indicates a typical signal to be observed in our measurements starting at e.g., $T_w = -5^\circ\text{C}$. At this temperature, only one phase of H₂O is initially present. Hence, the signal, denoted "ICE", is monitored first, Eq. (2). It exists as long as the sensor temperature does not approach $T(t) = 0^\circ\text{C}$. This case is identical to the limit $s(t) \rightarrow 0$, Eq. (30). From slope and intercept of the straight line (THS signal "L1" in Fig. 9, THW signal "L1a" in Fig. (12)), λ_s and a_s of ice can be calculated.

With the start of melting, the signal, denoted "ice-water" is observed. Now, two phases are concurrently present, the temperature profile within the liquid phase, T_L is established beginning at T_M . The interface is located at $r = s(t) > r_0$ for a THW and $r = s(t) > D$ for a THS experiment. Hence, after a transformation in time by the melt-lag Δt (cf. e.g., Figs. 9 and 12), the temperature of the sensor, $T(r_0, t - \Delta t)$, is specified by Eq. (25). Δt is the period to account for the time required to form a film of water around the sensor. From the slope of the straight line (THS signal "L2" in Fig. 9, THW signal "L1b" in Fig. (12)), λ_L of water can be calculated. The thermal diffusivity a_L of water can only be derived from the intercept of the lines mentioned when the latent heat is known. Or, vice versa, the latent heat of melting can be calculated with the knowledge of a_L .

4.2.2. Evaluation of Dual Sensor Signals

In the single sensor experiments only the cases $s(t) \rightarrow 0$ and $0 < r < s(t)$ (cf. Fig. 1) can be observed. In order to monitor all five cases mentioned above (cf. sect. 2.1.), a second temperature sensor, the "cold wire" was used at $r = r_1$ in conjunction with the hot wire. Now, the missing situations $s(t) < r < \infty$, $s(t) \rightarrow \infty$, and $s(t) = r_1$ (cf. Fig. 1) can be realized too. The cold wire signal of a bounded sample (radius R_0) is practically limited in time by the same restriction as the hot wire signal, Eq. (16): $t_{\max} < u R_0^2 / a$. However, there is a certain delay in time depending on the mutual distance of both wires, r_1 . This propagation delay, $\Delta t_{1-2} = t_{2\max} - t_{1\max}$, can be derived as e.g., $\Delta t_{1-2} = 581 \text{ s} - 373 \text{ s} = 208 \text{ s}$ from Fig. 12.

The first of the above mentioned cases, $s(t) \rightarrow 0$, is valid for ice. From slope and intercept, λ_s and a_s can be determined. This case is represented in Fig. 12, curve 2 and Fig. 13, curve 1. The latter diagram comprises all three typical cold wire signals, obtained from three different runs.

The fifth situation, the other limiting case $s(t) \rightarrow \infty$, is shown in Fig. 13, curve 3. Here, the transport properties of water can be derived from the signal.

The second and third cases, $0 < r < s(t)$, $s(t) < r < \infty$, respectively, can be seen from Fig. 13, curve 2a and curve 2c, respectively. Curve 2b is associated to the phase transition, $s(t) = r_1$, the fourth case. Surprisingly, in contrast to the THS signals, the THW signals of the hot and the cold wires show a "step" (Figs. 12 and 13: dotted rectangles) at the phase transition temperature. This characteristic behavior is not completely understood yet.

4.2.3. Results

The single phase experiments demonstrate that a simple THS instrument can be applied to measure the thermal conductivity not only of solids but also of fluids. The uncertainty compares to THW instruments which, however, are much more complicated to set up and to operate. The onset of convection is later for a THS than for a THW instrument, providing the same experimental conditions.

As a first result of the dual phase experiments using both transient techniques mentioned, the thermal transport properties λ_s and a_s for ice and λ_L for water can be obtained from one single run. These values differ only slightly ($\pm 1\%$) from those furnished by the single phase experiments. With the additional knowledge of a_L the volumetric latent heat of melting, ρH , of H_2O and the constant δ for the actual experiment can be calculated. For H we found 300 kJ/kg which is a fairly good value ([11]: 333 kJ/kg). For e.g., the THS signal depicted in Fig. 9, δ is

determined to be 0.48. From this value, the time dependent position of the interface, $s(t)$, between the two phases can be calculated.

A second result of the dual phase measurements is that the results are in complete agreement with the underlying theory.

5. SUMMARY

For the first time composite THW and THS signals have been observed which are monitored while the sample, H_2O , undergoes a phase transition from the solid to the liquid state. The apparatus used for these investigations is straightforward and simple to operate. Concerning the measured thermal conductivities of both phases, the results are in excellent agreement with those from literature. The value obtained for the latent heat is fairly good. However, till now THS is not the method of choice to precisely measure the thermal diffusivity of fluids.

It has been shown, that such experimental investigations can generally provide useful information for a lot of engineering applications like the melting of frozen food, thermal energy storage, or casting and welding of plastics.

REFERENCES

1. S. E. Gustafsson, E. Karawacki, and M. N. Khan, *J. Phys. D* **12**:1411 (1979)
2. S. E. Gustafsson, *Z. Naturforschg.* **22a**:1005 (1967)
3. S. E. Gustafsson, N. O. Hallig, and R. A. E. Kjellander, *Z. Naturforschg.* **23a**:682 (1968)
4. S. E. Gustafsson, E. Karawacki, and M.N. Khan, *J. Phys. D. Appl. Phys.* **12**:1411 (1979)
5. S. E. Gustafsson, E. Karawacki, and M.N. Khan, *J. Appl. Phys.* **52**:2596 (1981)
6. U. Groß, Y. W. Song, and E. Hahne, *Fluid Phase Equilibria* **76**: 273 (1992)
7. W. A. Wakeham, A. Nagashima, and J. V. Sengers, in *Measurement of the Transport Properties of Fluids, Vol. III*, Blackwell Scientific Publications, Oxford (1992)
8. A. I. Johns, A. C. Scott, J. T. R. Watson, D. Ferguson, and A. A. Clifford, *Phil. Trans. R. Soc. Lond. A* **325**:295 (1988)
9. U. Hammerschmidt, in *Proceedings 24th Int. Thermal Cond. Conf.*, Pittsburgh (1997)
10. W. Sabuga and U. Hammerschmidt, *Int. J. Thermophys.* **16**:557 (1995)
11. Y. S. Touloukian, R. W. Powell, C. Y. Ho, and P. G. Klemens, in *Thermophysical Properties of Materials*, Plenum Press, New York (1970)
12. E. H. Ratcliffe, *Phil. Mag.* **7**:1197 (1962)
13. M. L. V. Ramirez, C. A. Nieto de Castro, Y. Nagasaka, A. Nagashima, M. J. Assael, and W.A. Wakeham, *J. Phys. Chem. Ref. Data* **24**:1377 (1995)
14. U. Hammerschmidt and W. Sabuga, *Int. J. Thermophys.* **21**:217 (2000)
15. J. J. Healy, J. J. de Groot, and J. Kestin, *Physica* **82C**:392 (1976)
16. R. J. Model and U. Hammerschmidt, to be published at 6th Int. Conf. on Advanced Computational Methods in Heat Transfer, Heat Transfer 2000, Madrid, Spain, 26.-28. June 2000
17. Stefan, J., *Annalen der Physik und Chemie*, 42:269 (1891)
18. Neumann, F., lectures (1912)
19. Özisik, M. N., in *Heat Conduction*, 2nd edition, John Wiley and Sons Inc., New York (1993)
20. D. W. James, *J. Mat. Sci.* **3**:540 (1968)

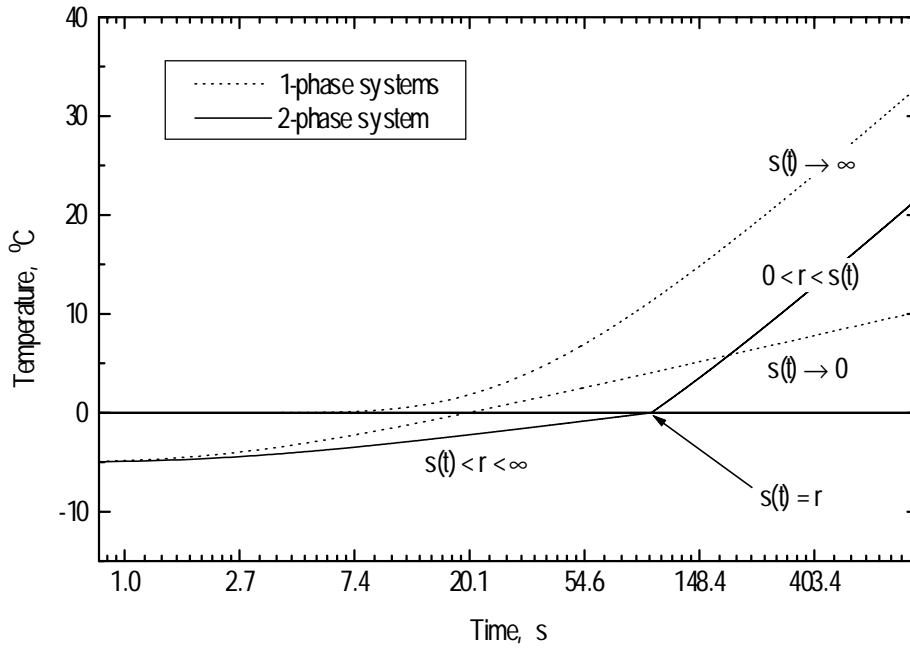


Fig. 1: Calculated temperature excursion for a solid and a liquid one-phase system and a two-phase system, the latter one during phase change (see text). $s(t)$ denotes the time dependent position of the phase boundary relative to the temperature station at r in cylindrical geometry.

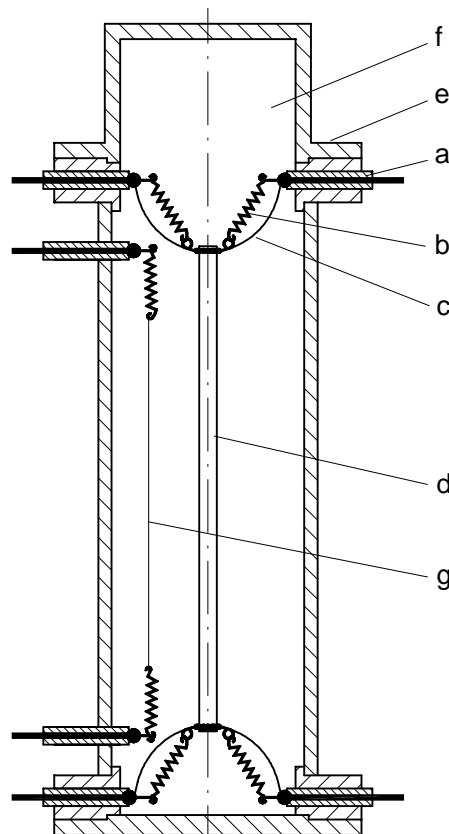


Fig. 2: Section through the PTB stainless steel THS/THW cell: **a** lead-through **b** tensioning spring **c** flexible potential or current lead **d** strip (or wire) **e** flange **f** excess volume (lid) **g** "cold wire"

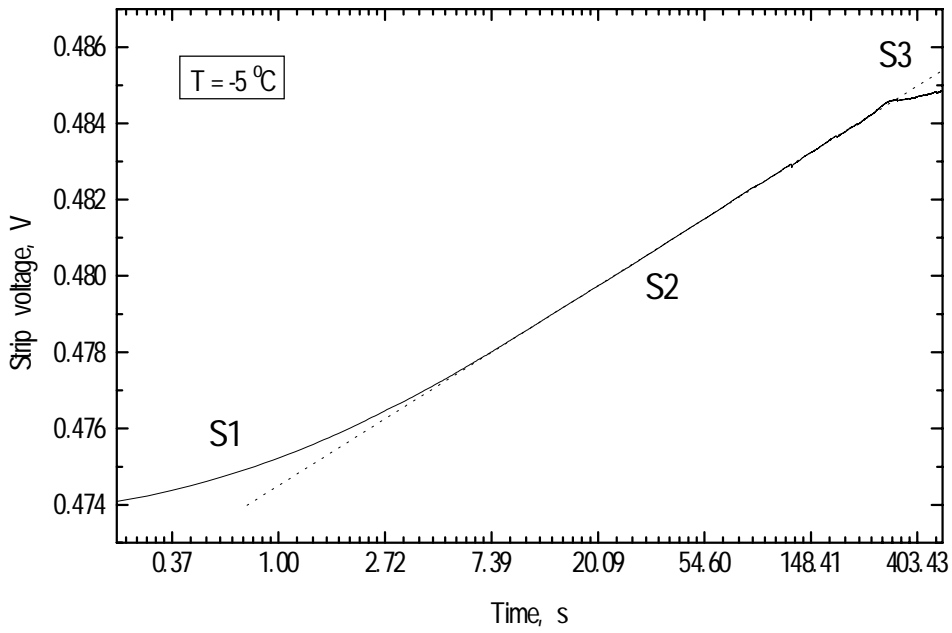


Fig. 3: Typical linearized THS voltage signal for ice (see text).

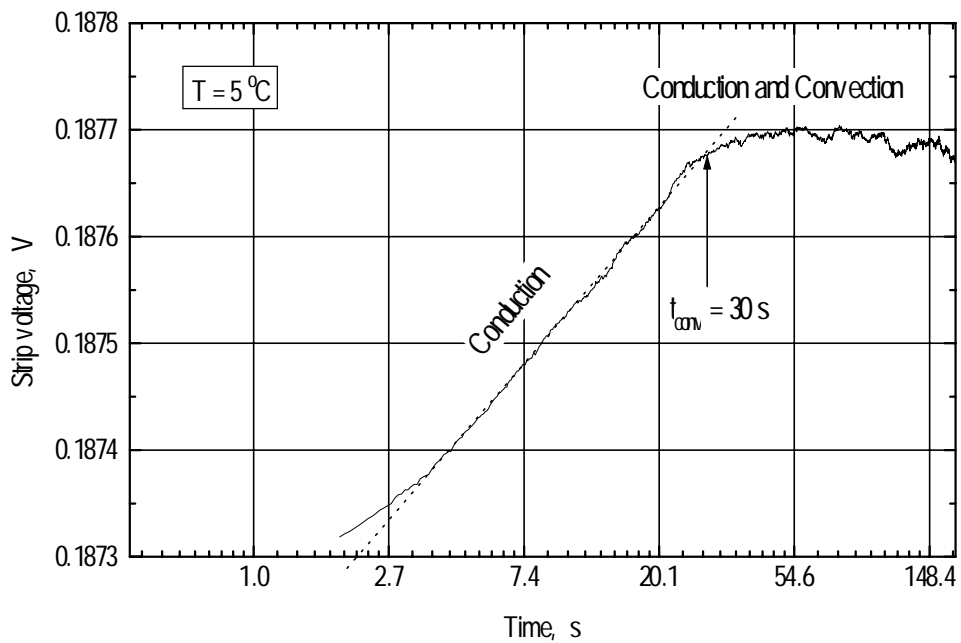


Fig. 4: Linearized THS voltage signal measured on water disturbed by convection for times above 30 s.

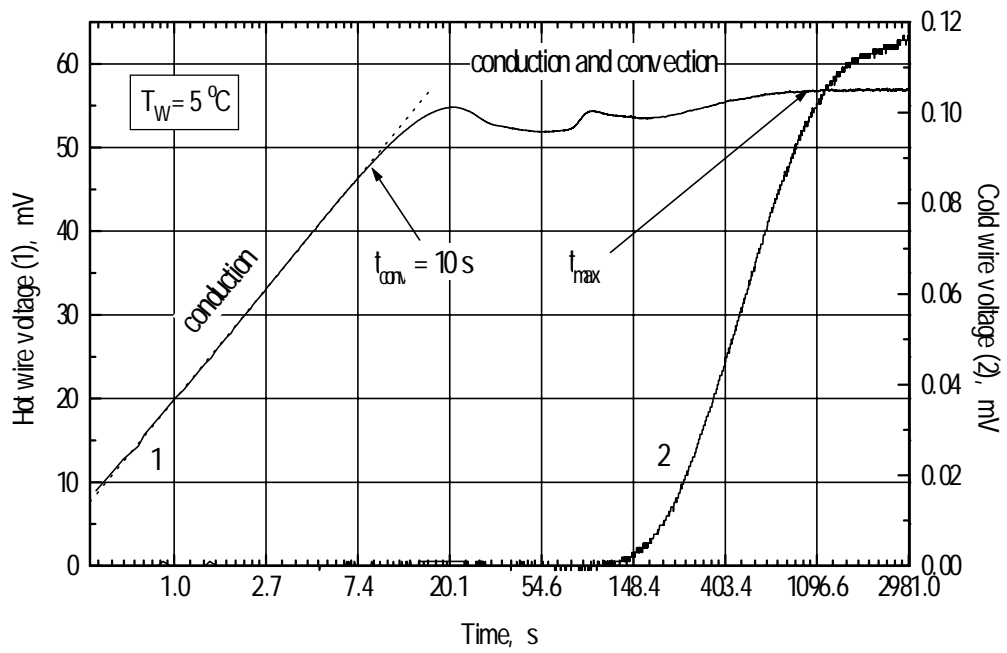


Fig. 5: Linearized THW voltage signal (curve 1) measured on water disturbed by convection for times above 10 s. Curve 2 represents the undisturbed "cold wire" voltage signal obtained simultaneously. t_{max} indicates the upper end of the measurement interval (see text).

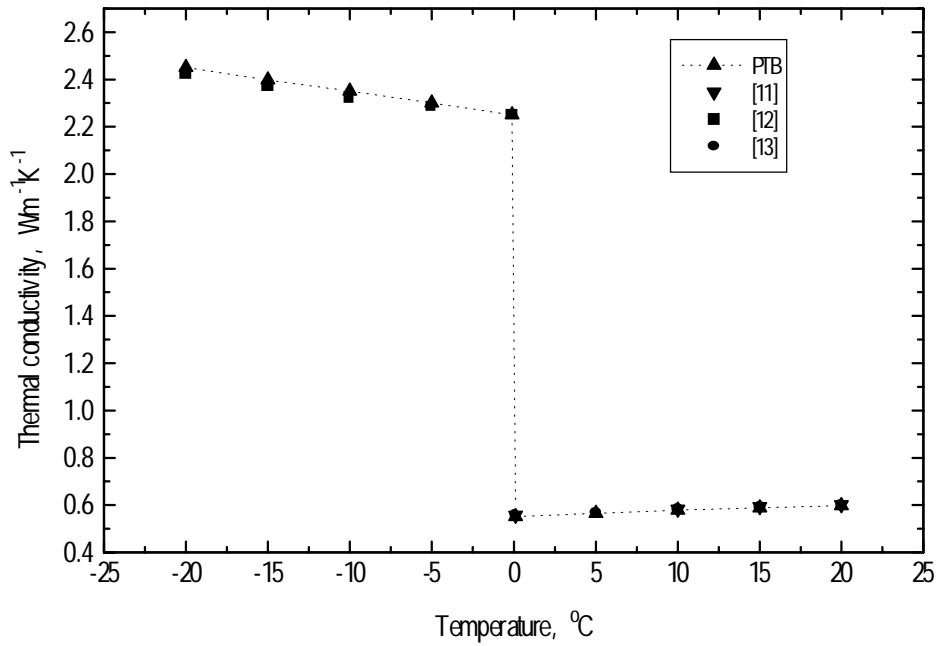


Fig. 6: Thermal conductivity of solid and liquid H₂O vs temperature as measured by the THS method [PTB], the THW method [12], [13] and a Guarded hot plate apparatus [11].

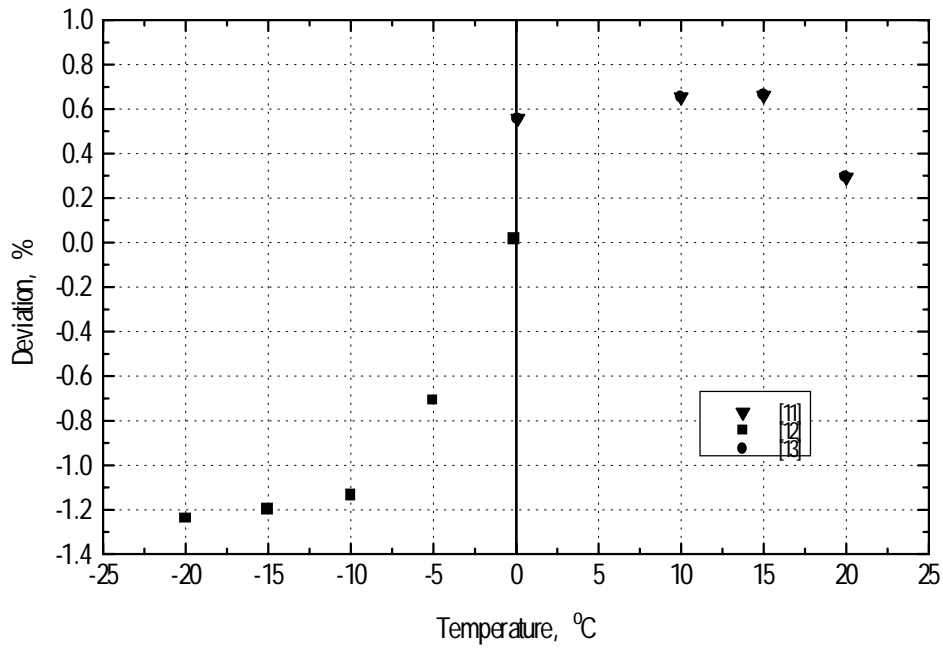


Fig. 7: Deviations of data sets selected (see text) from PTB THS data (baseline) on the thermal conductivity of H₂O (cf. Fig. 6).

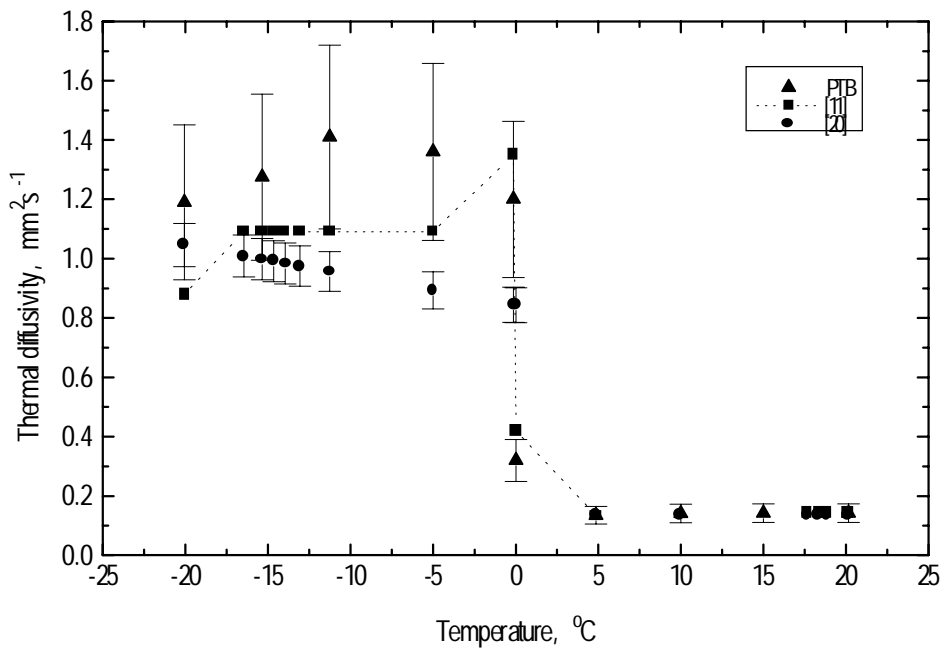


Fig. 8: Thermal diffusivity of solid and liquid H₂O vs temperature as measured by the THS method [PTB], the THW [11] and the Angström methods [20] (see text).

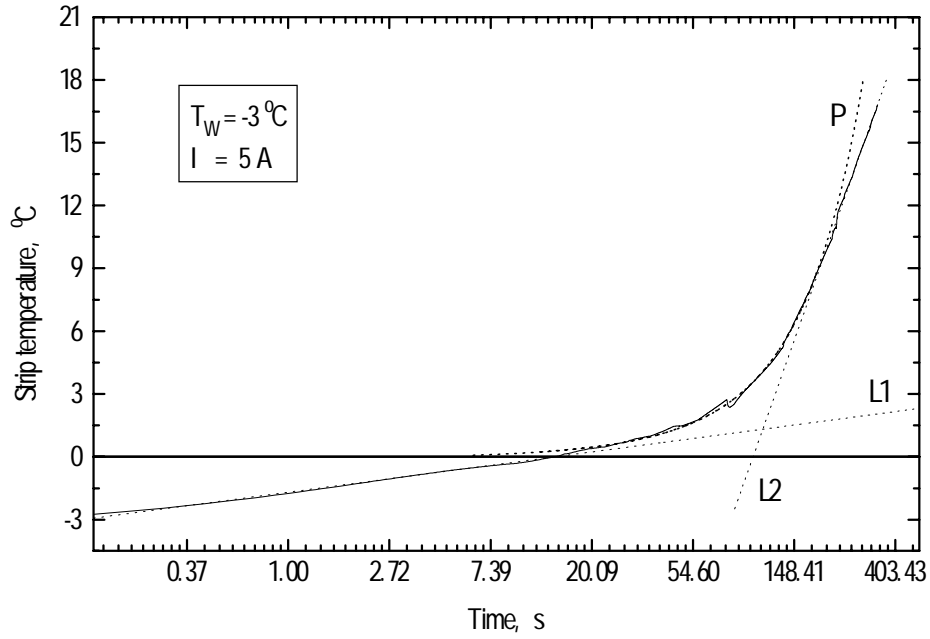


Fig. 9: Composite THS temperature signal for a solid-liquid phase transition of H_2O . "L1" and "L2" are linear fits while "P" is a quadratic polynomial fit.

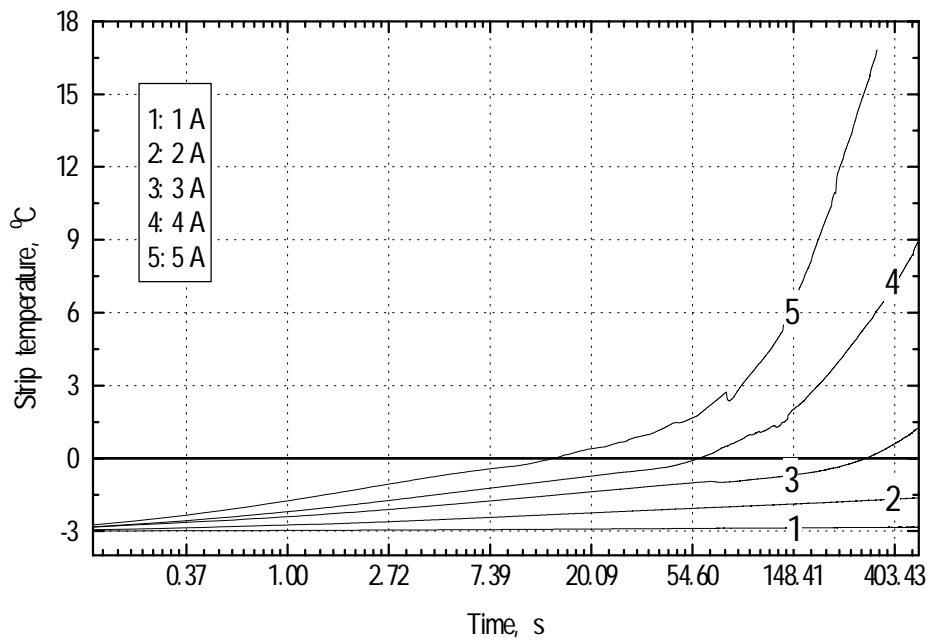


Fig. 10: Composite THS temperature signals measured with different electric currents fed to the strip. Curves 1 ... 5 are obtained for solid-liquid phase transitions of H_2O .

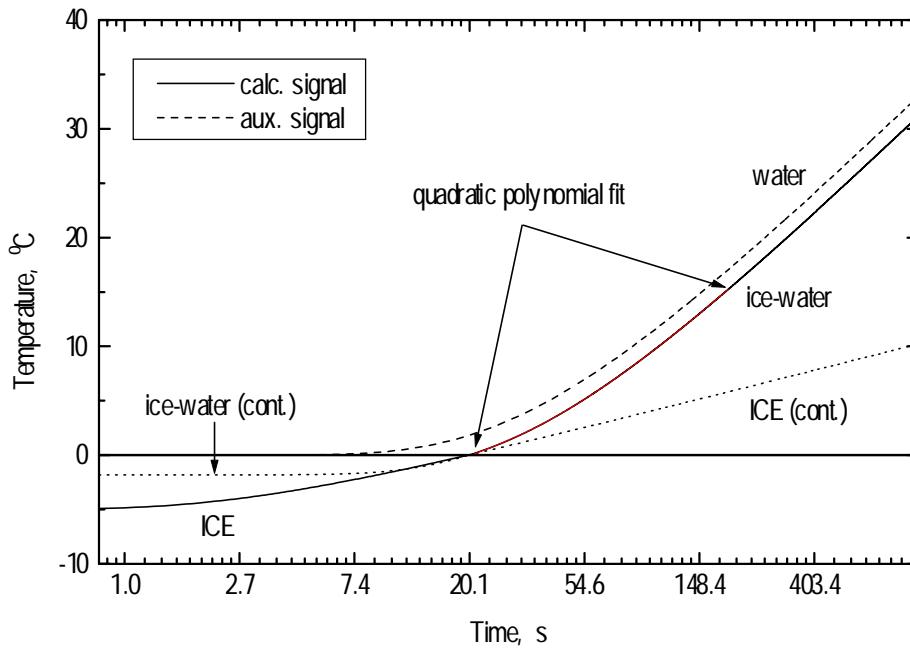


Fig. 11: Calculated temperature vs time curves for different phase conditions of H₂O during a phase change experiment (see text).

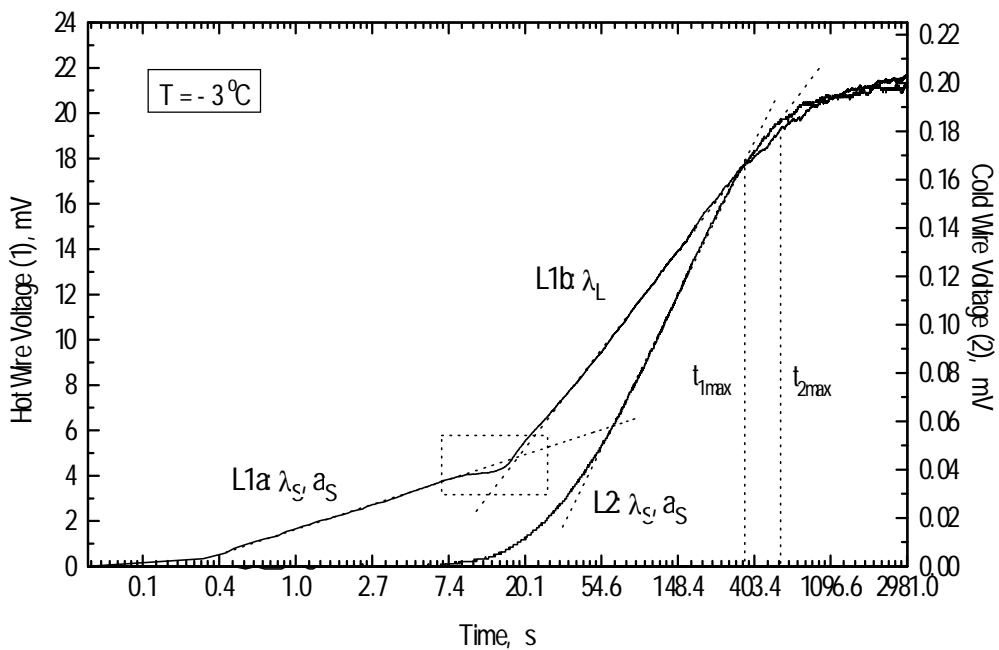


Fig. 12: Composite THW voltage signal for a solid-liquid phase transition of H₂O (curve 1). Curve 2 represents the "cold wire" voltage signal monitored simultaneously (see text).

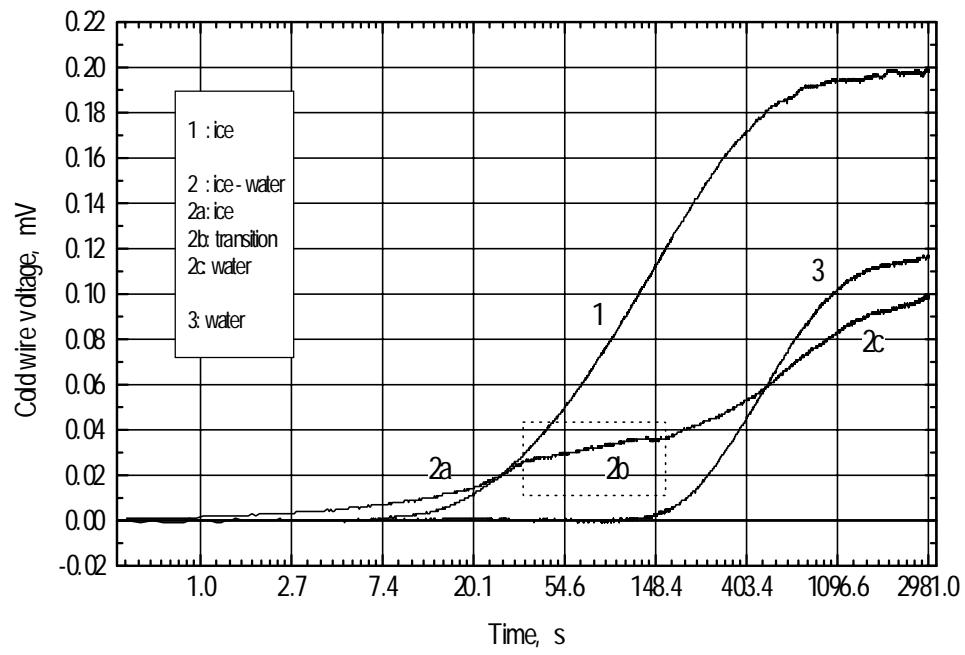


Fig. 13: "Cold wire" voltage signals from three different runs (1, 2, and 3) on the solid-liquid phase transition of H₂O (see text).